



## Abstract

Chemical and physical properties of individual ambient aerosol particles can vary greatly, so measuring the chemical composition at the single-particle level is essential for understanding atmospheric sources and transformations. Here we describe 46 days of single-particle measurements of atmospheric particles using a time-of-flight aerosol mass spectrometer coupled with a light scattering module (LS-ToF-AMS). The light scattering module optically detects particles larger than 180 nm vacuum aerodynamic diameter (130 nm geometric diameter) (with size resolution of 5–10 defined as  $d/\Delta d$  at full width at half maximum) before they arrive at the chemical mass detector and then triggers the saving of single-particle mass spectra. 271 641 particles were detected and sampled during 237 h of sampling in single particle mode. By comparing the timing of light scattering and chemical ion signals for each particle, particle types were classified and their number fractions determined as follows: prompt vaporization (49%), delayed vaporization (7%), and null (44%). LS-ToF-AMS provided the first direct measurement of the size-resolved collection efficiency (CE) of ambient particles, with an approximate 50% number-based CE for particles above detection limit. Prompt and delayed vaporization particles (147 357 particles) were clustered based on similar organic mass spectra (using *K*-means algorithm) to result in three major clusters: highly oxidized particles (dominated by  $m/z$  44), relatively less oxidized particles (dominated by  $m/z$  43), and particles associated with fresh urban emissions. Each of the three organic clusters had limited chemical properties of other clusters, suggesting that all of the sampled organic particle types were internally mixed to some degree; however, the internal mixing was never uniform and distinct particle types existed throughout the study. Furthermore, the single particle mass spectra and diurnal variations of these clusters agreed well with mass-based components identified (using factor analysis) from simultaneous ensemble-averaged measurements, supporting the connection between ensemble-based factors and atmospheric particle sources and

AMTD

5, 3047–3077, 2012

### Organics typed by single particle measurements

S. Liu et al.

Title Page

Abstract

Introduction

Conclusions

References

Tables

Figures

◀

▶

◀

▶

Back

Close

Full Screen / Esc

Printer-friendly Version

Interactive Discussion



processes. Measurements in this study illustrate that LS-ToF-AMS provides unique information about organic particle types by number as well as mass.

## 1 Introduction

Rapid measurements are needed to accurately quantify atmospheric particle sources and compositions and to study their transformations. The Aerosol Mass Spectrometer (AMS) is one fast-developing and widely used technique used for monitoring size and composition of submicron particles in real time (Jayne et al., 2000). Quantified species include nonrefractory organic mass (OM), sulfate, nitrate, ammonium, and chloride. Recent developments enable separation of ions that are slightly different in mass and overlap in unit-mass spectrum by replacing the quadrupole mass detector (in Q-AMS) with a compact time-of-flight mass spectral detector (C-ToF-AMS), as described in Drewnick et al. (2005), and a high resolution time-of-flight mass spectrometer (HR-ToF-AMS), described in DeCarlo et al. (2006). The ToF-AMS collects signals from the composition of ensembles of particles in each chopper cycle (143-Hz frequency). The single particle mode in the ToF-AMS operation is typically turned off during field measurements to conserve data storage and processing time. The only published analysis utilizing this mode came from field measurements made by Drewnick et al. (2005), whereby single-particle mass spectra were acquired several times, each for a few minutes. These single-particle spectra were used to investigate internal and external mixing properties of submicron particles. Cross et al. (2007, 2009) advanced the AMS by coupling a light scattering module (LS-ToF-AMS) in which particles are optically detected by a laser before they reach the vaporizer. Particle light scattering signals triggered the saving of single-particle mass spectra, which considerably enhanced data-saving efficiency. The LS-ToF-AMS was successfully deployed during the MILAGRO (Megacity Initiative: Local and Global Research Observations) 2006 field campaign for a 75-h sampling period (Cross et al., 2009), demonstrating its unique ability to provide insights into the atmospheric transformations of ambient particles.

### Organics typed by single particle measurements

S. Liu et al.

Title Page

Abstract

Introduction

Conclusions

References

Tables

Figures



Back

Close

Full Screen / Esc

Printer-friendly Version

Interactive Discussion





**Organics typed by  
single particle  
measurements**

S. Liu et al.

Title Page

Abstract

Introduction

Conclusions

References

Tables

Figures

◀

▶

◀

▶

Back

Close

Full Screen / Esc

Printer-friendly Version

Interactive Discussion



not influence ToF-AMS performance but rather physically identifies all particles (both nonrefractory and refractory) that reach the vaporizer and are larger than its detection limit, thereby providing substantially more information about single particles. During the entire campaign, the LS-ToF-AMS was operated in the “MS mode” (measures ensemble average chemical composition), “PToF mode” (particle-time-of-flight, provides size-resolved chemical composition for ensemble average), and “LS mode” (acquires single-particle mass spectrum) for 120, 120 and 80 s of every ~5 min.

Briefly, the LS-ToF-AMS has five major components: aerosol sampling inlet, particle time-of-flight chamber, light scattering module for single particle detection, particle vaporization and ionization chamber, and in this case, a high resolution time-of-flight mass spectrometer. Aerosols sampled through a 100- $\mu\text{m}$  critical orifice are focused by a series of aerodynamic lenses, forming a narrow ( $\sim 1$  mm diameter) and highly collimated particle beam. Focused particles are transmitted under high vacuum ( $\sim 10^{-5}$  Pa) through a laser beam for optical detection to the vaporization and ionization chamber, where they impact a heated surface ( $\sim 600^\circ\text{C}$ ). The nonrefractory fractions of the particles are flash vaporized and ionized by electron impact. Orthogonally extracted ions are subsequently analyzed by a time-of-flight detector, which generates a complete mass spectrum at each extraction. The detection process is fast enough ( $\sim 100\ \mu\text{s}$ ), compared to the traveling time ( $\sim 5$  ms) of the particles in the particle-sizing chamber, to allow correlated measurements of single particle light scattering and chemical compositions. A rotating chopper placed at the front of the particle-sizing chamber chops the particle beam and sets the starting time of particle flight. By measuring particle flight time between the mechanical chopper and the light scattering laser and thermal vaporizer, particle vacuum aerodynamic diameters ( $d_{va}$ ) can be determined from a calibration curve, which relates particle flight time to particle size for atomized ammonium nitrate particles of known sizes. In this study, geometric diameter ( $d_g$ ) is calculated using  $d_{va}$  and particle density ( $d_g = d_{va}/\rho$ ), assuming spherical particles. The density ( $1.4\ \text{g cm}^{-3}$ ) was derived by comparing AMS-measured mass size distribution with DMA-measured volume size distribution detailed in Lars et al. (2012).

**Organics typed by  
single particle  
measurements**

S. Liu et al.

Title Page

Abstract

Introduction

Conclusions

References

Tables

Figures



Back

Close

Full Screen / Esc

Printer-friendly Version

Interactive Discussion



The laser used for optical detection was a 405 nm continuous wave 50 mW laser (CrystaLaser, LC BCL-050-405). In order to maximize the overlap of the laser and the particle beams, the laser beam was not focused (Cross et al., 2007). Light scattered by sampled particles are collected using an ellipsoidal mirror and detected with a photomultiplier tube. The current system differs from the LS-ToF-AMS used by Cross et al. (2009) in the mechanism used for detecting single particles and saving the optical and chemical information for each detected particle. The key technical improvements include (1) adding the detected light scattering signal to the chopper frequency signal for unambiguous correlation in time, where the chopper frequency is the fundamental clock for all ToF-AMS data acquisition, and (2) using an external comparator circuit to test for the presences of a single particle in the scattered light signal, using a user set threshold level. The comparator circuit triggers the saving of the mass spectral data. Once triggered, the DAQ reports individual mass spectra for the entire chopper period in which the LS event occurred (mass spectra obtained as a function of particle time-of-flight). This approach dramatically reduces the overhead associated with any data saving for events where there were no particles and eliminates the need to transfer the data from the DAQ board to the computer for software detection of particles.

An additional improvement to the LS-ToF-AMS used during this study is a light scattering particle counter that counts all of the threshold crossers observed by the external comparator circuit in the LS, PToF, and MS modes. This includes LS pulses for which single particle mass spectral data were not recorded due to the transfer and saving times. This counter provides a measure of the particle number concentration for all optically detected particles and allows for the accurate evaluation of the true duty cycle obtained by the LS mode and direct comparisons with independent aerosol instruments that measure particle number concentrations.

The limiting issues with the LS mode include the typically low duty cycles of the chopper and the overhead associated with transferring and saving the mass spectral data for single particles (Kimmel et al., 2011). The chopper used during this study had a 0.02 duty cycle and operated at a frequency of 143 Hz. During the transferring



**Organics typed by  
single particle  
measurements**

S. Liu et al.

Title Page

Abstract

Introduction

Conclusions

References

Tables

Figures



Back

Close

Full Screen / Esc

Printer-friendly Version

Interactive Discussion



detected particle number concentrations to scanning Differential Mobility Analyzer (DMA)-measured number concentrations (Fig. 2), dropped below 100 % at 550 nm  $d_{va}$  (393 nm  $d_g$ ) and below 50 % at 430 nm  $d_{va}$  (307 nm  $d_g$ ). In comparison, the size that corresponds to 50 % optical detection efficiency, derived from LS-coupled Q-AMS system in the laboratory by Cross et al. (2007), was 240 nm  $d_g$  – 22 % lower than 307 nm  $d_g$ , suggesting that the alignment of LS-ToF-AMS used in this study was less optimized than that of the Cross et al. laboratory study. A group of particles with relatively high organic mass fractions ( $\sim 1$ ) and small sizes split from the majority of the particles (Fig. 1a). The split suggests particles that are dominated by organics had significantly lower diameter than internally mixed organic and inorganic particles (which had low organic fractions), likely because the organic-dominating particles were primary (directly emitted to the atmosphere) and of nonspherical shapes (i.e., black carbon fragments), resulting in smaller diameter than those of spherical particles (DeCarlo et al., 2004).

Total saved particles were scaled by overall chopper duty cycle to derive average particle number size distribution for this study. The overall duty cycle accounted for the 2 % chopper duty cycle, data transferring and saving duty cycle (0.62), and noise spike duty cycle (0.45). Figure 2 represents the first direct in situ measure of the particle number-based sampling efficiency of an AMS and comparison with simultaneous DMA number-based measurements. The light scattering signals indicate that particle sampling efficiency for particle sizes greater than 550 nm  $d_{va}$  (393 nm  $d_g$ ) is similar to the laboratory measurements for the aerodynamic inlet lens system, with decreasing transmission efficiency at larger particle sizes (Liu et al., 2007).

Low detection efficiency for small particles likely resulted from (i) widening of particle beam beyond the region of overlap of the particle and laser beams, (ii) low detection efficiency for small particles passing through the edges of the laser beam, and (iii) size detection limit of small particles by the laser. Comparison of LS-ToF-AMS- and DMA-measured particle total number concentration time series showed similar result, i.e., total number concentration of 400- to 1000-nm  $d_{va}$  (285- to 715-nm  $d_g$ ) particles agreed reasonably well (slope = 1.0 and  $R = 0.7$ ; Supplement), while total concentration of

200- to 400-nm  $d_{va}$  (140- to 285-nm  $d_g$ ) particles measured by LS-ToF-AMS was much lower.

In order to determine the timing of the chemical signals, a mass intensity profile (i.e., mass intensity quantified by the ToF-MS detector as a function of particle time-of-flight) is needed for each particle. The profile is the sum of profiles for all detected ion fragments (including organic and inorganic fragments) for each particle. Since the acquisition rate is faster than the particle vaporization time, several mass spectra are obtained during the ( $\sim 100$   $\mu$ s) particle vaporization event. These individual spectra are added to accumulate the total measured ion intensity for the single particle. However, adding fragments with low intensities can significantly lower the contrast between real and background signals. Additionally, background-related fragments  $m/z$  18 ( $H_2O^+$ ), 28 ( $N_2^+$ ), 32 ( $O_2^+$ ), and 39 ( $K^+$ ) can greatly mask real signals. Therefore, only the profiles of nonbackground high-intensity fragments were summed to construct a mass intensity profile for each particle.

Ensemble average concentrations (from MS mode) were used to estimate ion fragment abundance in single particles. Ten high-intensity ion fragments were selected for this campaign, including  $m/z$  15, 27, 30, 41, 43, 44, 46, 48, 55, 57, and 64. This list combined organic- and inorganic- (nitrate and sulfate) dominated fragments. Additionally, selected organic fragments were characteristics of specific particle types; for example,  $m/z$  44 is a tracer for oxygenated organic aerosols (OOA), and  $m/z$  57 typically represents hydrocarbon-like organic aerosols (HOA) (Zhang et al., 2005).

Timing of the optical signals was retrieved by locating the maximum light scattering intensity from the light scattering profile (i.e., light scattering intensity as a function of particle time-of-flight). After comparing the physical signal identifying particle arrival (time to detector calculated from the time of light scattering,  $T_{LS}$ ) to the chemical signal identifying particle arrival (time of mass spectrum,  $T_{MS}$ ), each single particle was classified into one of three discrete particle types: (1) “prompt,” for which the deviation of  $T_{MS}/T_{LS}$  from 1 was less than 20 % (i.e., particles optically and chemically detected at the expected time offset); (2) “delayed,” for which the deviation of  $T_{MS}/T_{LS}$  from 1 was

**Organics typed by  
single particle  
measurements**

S. Liu et al.

Title Page

Abstract

Introduction

Conclusions

References

Tables

Figures

◀

▶

◀

▶

Back

Close

Full Screen / Esc

Printer-friendly Version

Interactive Discussion



greater than 20 % (i.e.,  $T_{MS}$  significantly lagged  $T_{LS}$ ); and (3) “null,” for which optical signals were detected, but no significant chemical signals were observed. The criteria of insignificant chemical signals includes a minimum sum of chemical signals for the mass intensity profile of 100 ions.

Particle statistics associated with the three vaporization types (Table 2) show that prompt and null particles dominated, accounting for 46 % and 48 %, respectively, of saved particles, while delayed particles accounted for a 6 % fraction. The null particle fraction was comparable to that of the 51 % fraction identified from the Mexico City measurement (Cross et al., 2009), suggesting that the AMS vaporization-ionization may typically miss about 50 % of sampled particles (for particle diameters larger than 180 nm  $d_{va}$  or 130 nm  $d_g$ ), based on particle number. The mass-based collection efficiency (CE) of the AMS is dependent on particle composition and is higher for low-sulfate particles (Quinn et al., 2006; Matthew et al., 2008; Middlebrook et al., 2012). While the prompt particle (46 %) group points to a number-based CE of  $\sim 0.5$  for particles larger than 180 nm  $d_{va}$  (130 nm  $d_g$ ), smaller particles (<180 nm) may have had higher CE due to their near-zero sulfate content (Ahlm et al., 2012). Therefore, the number-based CE of 0.5 was lower compared to the average mass-based CE of 0.8, which was determined by scaling AMS mass to DMA-derived mass for particles of all sizes smaller than 1000 nm  $d_{va}$  (715 nm  $d_g$ ) (excluded masses of elemental carbon and dusts) (Ahlm et al., 2012). CEs ranged from 0.43 to 0.52 for particles larger than 180 nm  $d_{va}$  (130 nm  $d_g$ ), with peak values associated with 500–600 nm particles (Fig. 3). Particles in 800- to 1000-nm  $d_{va}$  (570- to 715-nm  $d_g$ ) had the lowest CEs, likely due to enriched dust components in this size range (Silva et al., 2000) that were not vaporized by the AMS.

### 3.2 Organic particle types identified from cluster analysis

Prompt and delayed particles that had significant mass spectrum signals were used for cluster analysis. The  $K$ -means clustering algorithm, applied to the 147 357 single-particle organic mass spectra, divides spectra into  $K$  clusters such that the sum of

## Organics typed by single particle measurements

S. Liu et al.

Title Page

Abstract

Introduction

Conclusions

References

Tables

Figures

◀

▶

◀

▶

Back

Close

Full Screen / Esc

Printer-friendly Version

Interactive Discussion



**Organics typed by  
single particle  
measurements**

S. Liu et al.

Title Page

Abstract

Introduction

Conclusions

References

Tables

Figures

◀

▶

◀

▶

Back

Close

Full Screen / Esc

Printer-friendly Version

Interactive Discussion



squares of the distances between the spectra and their corresponding cluster centroid is minimized (Hartigan and Wong, 1979). Spectra were normalized before clustering such that the sum of intensities for each mass spectrum was 1. In order to identify organic particle types, only organic fragments were included in the cluster analysis.  $K$  values of 2 to 12 (varying by 1) were tested. For each run, 10 sets of random cluster centroids were iterated. Using  $K \leq 6$  resulted in one dominating cluster (containing ~75 % of particles used for clustering) with an average spectrum characterized by mixed types of marker fragments (e.g.,  $m/z$  44 for OOA and  $m/z$  55 for cooking organic aerosols), which indicated that particles in this cluster were not well separated; thus,  $K \leq 6$  solutions were not preferred. However, three major clusters were consistently identified from the  $K > 6$  clustering solutions, with each cluster associated with a distinct mass spectrum. Taken together, these particles accounted for 80 % of the particles. Each of the remaining clusters typically contained less than 5 % of the particles.

Cosine similarity is a useful tools for estimating mass spectrum similarity (Stein and Scott, 1994) and was therefore used here as a metric to measure the within-cluster and cross-cluster similarity of single-particle spectra. In brief, cosine similarity is the cosine of the angle between two vectors (where each vector represents a mass spectrum) and is calculated using the following equation:

$$\cos \theta = \frac{\mathbf{A} \cdot \mathbf{B}}{\|\mathbf{A}\| \cdot \|\mathbf{B}\|} = \frac{\sum_i^n A_i \times B_i}{\sqrt{\sum_i^n (A_i)^2} \times \sqrt{\sum_i^n (B_i)^2}} \quad (1)$$

where  $\|\mathbf{A}\|$  and  $\|\mathbf{B}\|$ , respectively, represent the magnitudes of vectors  $\mathbf{A}$  and  $\mathbf{B}$ , and  $\mathbf{A} \cdot \mathbf{B}$  denotes the dot product of  $\mathbf{A}$  and  $\mathbf{B}$ . Cosine similarity ranges from 0 to 1, with higher values representing smaller angles and higher similarity. The cosine similarity between each single particle spectrum and the three major cluster centroids (the average spectra) was calculated (Fig. 4). Spectra in Cluster I had significantly higher similarity (median value is  $>0.8$ ) to Cluster I centroid than Cluster II and III centroids

(Fig. 4a). In other words, the within-cluster similarity was far higher than the cross-cluster similarity for Cluster I spectra. In addition, the variability of the within-cluster similarity was lower than that of the cross-cluster similarity, suggesting good separation of Cluster I spectra. Similar results were found for Cluster II spectra (Fig. 4b).

5 Compared to Cluster I and Cluster II, the within-cluster similarity for Cluster III spectra had lower values (median value of 0.5) and greater variability (Fig. 4c). However, the within-cluster similarity was significantly higher than the cross-cluster similarity (99 % confidence level) for Cluster III spectra. The cosine similarity analysis also suggests that each cluster may have limited chemical properties of other clusters, indicating that  
10 particles were likely internally mixed but dominated by one type so they can be grouped by the dominant signatures.

The effects of single-particle size and organic mass fraction on the derived single-particle clusters were examined. The number of organic ions detected for each single-particle is a function of the organic mass fraction (for a given threshold of 100 ions  
15 described in Sect. 3.1) and particle size (larger particles produce more ions). Sulfate and nitrate, the major inorganic ions, were found to be independent of organic cluster types (Fig. 5), i.e., sulfate and nitrate, respectively, accounted for 16 % and 4 % of single-particle mass for each cluster (on average). To test the effects of organic mass fractions on the derived clusters, the *K*-means algorithm was applied to four subsets  
20 of the total 147 357 particles, which were composed of particles with organic mass fractions greater than 10 %, 20 %, 30 %, and 40 % of the total particle mass, respectively. Three major clusters were identified in each case. The cluster centroids were identical to the centroids of Clusters I to III, and the relative cluster sizes (number of particles in the cluster) were comparable to the sizes of Clusters I to III, indicating  
25 that the same single-particle clusters were identified. The effects of particle size on clustering results were tested by applying the *K*-means analysis to three subsets of the total particles, which were composed of particles larger than 300 nm, 400 nm, and 500 nm  $d_{va}$ , respectively. The same clusters (as Clusters I to III) were identified. That the inorganic-to-organic mass ratio and particle size did not affect the results of cluster

**Organics typed by  
single particle  
measurements**

S. Liu et al.

Title Page

Abstract

Introduction

Conclusions

References

Tables

Figures

◀

▶

◀

▶

Back

Close

Full Screen / Esc

Printer-friendly Version

Interactive Discussion



analysis indicated that the single-particle organic mass ions were sufficient for cluster analysis and the identified clusters were robust.

Examples of single-particle spectra for the three major clusters are shown in Fig. 5a. While the single-particle spectra exhibit large variability (Fig. 5b), the centroids for the three particle types (Fig. 6a) show that the Cluster I spectrum was characterized by a dominant peak at  $m/z$  44, comparable to that of LV-OOA (low-volatility OOA) components extracted from the positive matrix factorization (PMF) analysis in a number of field measurements (Ulbrich et al., 2009). This indicates that particles in this cluster were highly oxidized and associated with high O/C, which is consistent with the noon-high particle number concentration for Cluster I (Fig. 7). It is suggested that Cluster II particles, which had strong  $m/z$  43 signals and mass spectra resembling those of SV-OOA (semi-volatile OOA) components identified by Lanz et al. (2007), Ng et al. (2010), and Ulbrich et al. (2009), were relatively less oxidized SOA and, so, were likely associated with lower O/C than Cluster I particles. The number concentration of Cluster II particles increased at night, likely resulting from temperature-driven condensation of this particle type under low-temperature conditions as suggested in previous studies (Huang et al., 2011; Lanz et al., 2007), given daily temperature fluctuations of 10–20 °C over the course of the measurements. The average spectrum for Cluster III particles was characterized by  $m/z$  27, 41, 43, 55, 69, 29, and 57, in which  $m/z$  29 and 57 are markers for HOA and  $m/z$  27, 41, 55, and 69 are cooking organic aerosol (COA) tracers (He et al., 2010). This suggests that particles in Cluster III were produced by a mixture of different sources, possibly including local unoxidized vehicular emissions at night and cooking oils. The number concentration of Cluster III particles was high at night and continued until 1400 in the afternoon.

The organic particles that had nearly no sulfate or nitrate (Fig. 1a) were mostly in Cluster III (Fig. 1b). Specifically, mass concentration of these particles peaked at night and correlated to fragment  $C_4H_9^+$  ( $m/z$  57) with  $r$  of 0.72, suggesting that these particles were HOA-like and originated from nighttime sources, in which vehicular emissions could be significant. These HOA-like particles were likely associated with nonspherical

## Organics typed by single particle measurements

S. Liu et al.

Title Page

Abstract

Introduction

Conclusions

References

Tables

Figures

◀

▶

◀

▶

Back

Close

Full Screen / Esc

Printer-friendly Version

Interactive Discussion



black carbon cores, resulting in smaller diameter in the AMS measurements and causing the split in Fig. 1. A similar result was observed in Cross et al. (2009).

Size distributions of particle types (Fig. 2) show an increased number fraction of Cluster I type for particles larger than 300 nm  $d_{va}$  (215 nm  $d_g$ ). In contrast, Cluster III type dominated particles smaller than 400 nm  $d_{va}$  (285 nm  $d_g$ ). Compared to Cluster I and Cluster III particle types, Cluster II type was more evenly distributed across particle size. A likely explanation of size dependence of particle types is that oxidized particles (in Cluster I) formed by condensation of secondary vapors onto preexisting particles so that they grew bigger, whereas Cluster III particles were associated with fresh emissions in which particles were smaller. This is consistent with the split of particles in Fig. 1, with small and primarily organic particles dominated by Cluster III type (Fig. 1b).

### 3.3 Comparison of single-particle types with ensemble components

Cluster I, Cluster II, and Cluster III particle types broadly matched the OM components identified from ensemble factor analysis using PMF (Liu et al., 2012). Ensemble-based OM spectra were categorized into three groups according to their O/C values (calculated from the high resolution mass spectra using the method described by Aiken et al., 2007): Group I consisted of high O/C alkane and aromatic SOA components (O/C=0.63–0.68); Group II consisted of low O/C alkane and aromatic SOA components (O/C=0.27–0.36); and Group III was likely a mixture of cooking organic aerosol (COA), petroleum operation (PO) SOA, and local traffic and biogenic nighttime OA (NOA) components (O/C=0.00–0.20). The mass fractions of  $m/z$  44 ( $f_{44}$ ; an indicator of O/C (Aiken et al., 2008)) for Cluster I (23.1%), Cluster II (4.1%), and Cluster III (2%) reasonably agreed with the  $f_{44}$  for the ensemble-based Group I (19.6%), Group II (2.4%), and Group III (0.5%), respectively. Specifically, the Cluster I centroid correlated to the mass spectra for high O/C alkane and aromatic SOA components with an  $r$  of 0.96 and 0.92, respectively (Fig. 6). The mass fraction of Cluster I particles had a similar magnitude and diurnal cycle to that of the high O/C alkane SOA component (Fig. 8), supporting the consistency of Cluster I particles with high O/C components.

## Organics typed by single particle measurements

S. Liu et al.

Title Page

Abstract

Introduction

Conclusions

References

Tables

Figures

◀

▶

◀

▶

Back

Close

Full Screen / Esc

Printer-friendly Version

Interactive Discussion



**Organics typed by  
single particle  
measurements**

S. Liu et al.

Title Page

Abstract

Introduction

Conclusions

References

Tables

Figures



Back

Close

Full Screen / Esc

Printer-friendly Version

Interactive Discussion



The centroid for Cluster II particles correlated to that of the low O/C alkane SOA component with an  $r$  of 0.96. The Cluster III centroid correlated to the spectra for COA, PO SOA, and NOA components with an  $r$  of 0.86, 0.76, and 0.70, respectively. Correlation of the Cluster III centroid to the mass-weighted average spectrum for COA, PO SOA and NOA (Fig. 6b-iii) showed an  $r$  of 0.82. The mass fraction of Cluster III particles and the sum of ensemble-derived Group III components co-varied, with low fractions during daytime and increased abundance at night. There were some deviations in magnitude and timing of diurnal cycles for single-particle clusters and ensemble-derived components, likely arising from measurement uncertainties and internally mixed particles that were split between more than one cluster or assigned to one of the minor clusters (IV, V, VI). Good comparison between single particle clusters and ensemble factors confirmed that the factors reflected organic components of different origins and atmospheric processes.

#### 4 Concluding remarks

The LS-ToF-AMS was valuable for separating single particles with different organic chemical compositions in a 46-day field campaign. 271 641 single particles were optically detected and the chemical mass spectra saved and classified by comparison of the optical and chemical information, with a 46 % prompt (chemical and optical signals detected nearly simultaneously) fraction, a 48 % null (produced significant light scattering but insignificant mass spectrum signals, likely due to particle bounce) fraction, and a 6 % delayed particle fraction (chemical signals delayed relative to optical signals). Thus, the LS-ToF-AMS provided a direct measure of the collection efficiency (CE) of ambient particles, resulting in an approximate 50 % number-based CE for particles larger than 180 nm  $d_{va}$  (130 nm  $d_g$ ). This was lower than the overall mass-based CE of 0.8, likely due to higher CE for particles smaller than 180 nm  $d_{va}$  (130 nm  $d_g$ ) (which typically had lower ammonium sulfate and therefore bounced less in the vaporizer).



with material reported herein is not to be construed as actual or implied endorsement of such products.

## References

- Ahlm, L., Liu, S., Day, D. A., Russell, L. M., Weber, R., Gentner, D. R., Goldstein, A. H., DiGangi, J. P., Henry, S. B., Keutsch, F. N., VandenBoer, T. C., Markovic, M. Z., Murphy, J. G., Ren, X., and Scheller, S.: Formation and growth of ultrafine particles from secondary sources in bakersfield, california, *J. Geophys. Res.-Atmos.*, 117, D00V08, doi:10.1029/2011JD017144, 2012.
- Aiken, A. C., DeCarlo, P. F., and Jimenez, J. L.: Elemental analysis of organic species with electron ionization high-resolution mass spectrometry, *Anal. Chem.*, 79, 8350–8358, 2007.
- Aiken, A. C., Decarlo, P. F., Kroll, J. H., Worsnop, D. R., Huffman, J. A., Docherty, K. S., Ulbrich, I. M., Mohr, C., Kimmel, J. R., Sueper, D., Sun, Y., Zhang, Q., Trimborn, A., Northway, M., Ziemann, P. J., Canagaratna, M. R., Onasch, T. B., Alfarra, M. R., Prevot, A. S. H., Dommen, J., Duplissy, J., Metzger, A., Baltensperger, U., and Jimenez, J. L.: O/C and OM/OC ratios of primary, secondary, and ambient organic aerosols with high-resolution time-of-flight aerosol mass spectrometry, *Environ. Sci. Technol.*, 42, 4478–4485, 2008.
- Allan, J. D., Bower, K. N., Coe, H., Boudries, H., Jayne, J. T., Canagaratna, M. R., Millet, D. B., Goldstein, A. H., Quinn, P. K., Weber, R. J., and Worsnop, D. R.: Submicron aerosol composition at trinidad head, california, during itct 2k2: Its relationship with gas phase volatile organic carbon and assessment of instrument performance, *J. Geophys. Res.-Atmos.*, 109, D23S24, doi:10.1029/2003JD004208, 2004.
- Cross, E. S., Slowik, J. G., Davidovits, P., Allan, J. D., Worsnop, D. R., Jayne, J. T., Lewis, D. K., Canagaratna, M., and Onasch, T. B.: Laboratory and ambient particle density determinations using light scattering in conjunction with aerosol mass spectrometry, *Aerosol Sci. Tech.*, 41, 343–359, 2007.
- Cross, E. S., Onasch, T. B., Canagaratna, M., Jayne, J. T., Kimmel, J., Yu, X.-Y., Alexander, M. L., Worsnop, D. R., and Davidovits, P.: Single particle characterization using a light scattering module coupled to a time-of-flight aerosol mass spectrometer, *Atmos. Chem. Phys.*, 9, 7769–7793, doi:10.5194/acp-9-7769-2009, 2009.

## Organics typed by single particle measurements

S. Liu et al.

Title Page

Abstract

Introduction

Conclusions

References

Tables

Figures



Back

Close

Full Screen / Esc

Printer-friendly Version

Interactive Discussion



**Organics typed by  
single particle  
measurements**

S. Liu et al.

Title Page

Abstract

Introduction

Conclusions

References

Tables

Figures

◀

▶

◀

▶

Back

Close

Full Screen / Esc

Printer-friendly Version

Interactive Discussion



DeCarlo, P. F., Slowik, J. G., Worsnop, D. R., Davidovits, P., and Jimenez, J. L.: Particle morphology and density characterization by combined mobility and aerodynamic diameter measurements, Part 1: Theory, *Aerosol Sci. Tech.*, 38, 1185–1205, 2004.

DeCarlo, P. F., Kimmel, J. R., Trimborn, A., Northway, M. J., Jayne, J. T., Aiken, A. C., Gonin, M., Fuhrer, K., Horvath, T., Docherty, K. S., Worsnop, D. R., and Jimenez, J. L.: Field-deployable, high-resolution, time-of-flight aerosol mass spectrometer, *Anal. Chem.*, 78, 8281–8289, 2006.

Drewnick, F., Hings, S. S., DeCarlo, P., Jayne, J. T., Gonin, M., Fuhrer, K., Weimer, S., Jimenez, J. L., Demerjian, K. L., Borrmann, S., and Worsnop, D. R.: A new Time-of-Flight Aerosol Mass Spectrometer (ToF-AMS) – instrument description and first field deployment, *Aerosol Sci. Tech.*, 39, 637–658, 2005.

Gard, E., Mayer, J. E., Morrical, B. D., Dienes, T., Ferguson, D. P., and Prather, K. A.: Real-time analysis of individual atmospheric aerosol particles: design and performance of a portable atofms, *Anal. Chem.*, 69, 4083–4091, 1997.

Hartigan, J. A. and Wong, M. A.: A *K*-means clustering algorithm, *Appl. Stat.*, 28, 100–108, doi:10.2307/2346830, 1979.

He, L.-Y., Lin, Y., Huang, X.-F., Guo, S., Xue, L., Su, Q., Hu, M., Luan, S.-J., and Zhang, Y.-H.: Characterization of high-resolution aerosol mass spectra of primary organic aerosol emissions from Chinese cooking and biomass burning, *Atmos. Chem. Phys.*, 10, 11535–11543, doi:10.5194/acp-10-11535-2010, 2010.

Huang, X.-F., He, L.-Y., Hu, M., Canagaratna, M. R., Kroll, J. H., Ng, N. L., Zhang, Y.-H., Lin, Y., Xue, L., Sun, T.-L., Liu, X.-G., Shao, M., Jayne, J. T., and Worsnop, D. R.: Characterization of submicron aerosols at a rural site in Pearl River Delta of China using an Aerodyne High-Resolution Aerosol Mass Spectrometer, *Atmos. Chem. Phys.*, 11, 1865–1877, doi:10.5194/acp-11-1865-2011, 2011.

Jayne, J. T., Leard, D. C., Zhang, X. F., Davidovits, P., Smith, K. A., Kolb, C. E., and Worsnop, D. R.: Development of an aerosol mass spectrometer for size and composition analysis of submicron particles, *Aerosol Sci. Tech.*, 33, 49–70, 2000.

Johnston, M. V. and Wexler, A. S.: Ms of individual aerosol particles, *Anal. Chem.*, 67, A721–A726, doi:10.1021/ac00119a002, 1995.

Kimmel, J. R., Farmer, D. K., Cubison, M. J., Sueper, D., Tanner, C., Nemitz, E., Worsnop, D. R., Gonin, M., and Jimenez, J. L.: Real-time aerosol mass spectrometry with millisecond resolution, *Int. J. Mass Spectrom.*, 303, 15–26, 2011.

**Organics typed by  
single particle  
measurements**

S. Liu et al.

Title Page

Abstract

Introduction

Conclusions

References

Tables

Figures



Back

Close

Full Screen / Esc

Printer-friendly Version

Interactive Discussion



- Lake, D. A., Tolocka, M. P., Johnston, M. V., and Wexler, A. S.: Mass spectrometry of individual particles between 50 and 750 nm in diameter at the baltimore supersite, *Environ. Sci. Technol.*, 37, 3268–3274, 2003.
- Lanz, V. A., Alfara, M. R., Baltensperger, U., Buchmann, B., Hueglin, C., and Prévôt, A. S. H.: Source apportionment of submicron organic aerosols at an urban site by factor analytical modelling of aerosol mass spectra, *Atmos. Chem. Phys.*, 7, 1503–1522, doi:10.5194/acp-7-1503-2007, 2007.
- Laskin, A. and Cowin, J. P.: Automated single particle sem/edx analysis of submicrometer particles down to 0.1  $\mu\text{m}$ , *Anal. Chem.*, 73, 1023–1029, 2001.
- Li, W. J., Zhou, S. Z., Wang, X. F., Xu, Z., Yuan, C., Yu, Y. C., Zhang, Q. Z., and Wang, W. X.: Integrated evaluation of aerosols from regional brown hazes over Northern China in winter: concentrations, sources, transformation, and mixing states, *J. Geophys. Res.-Atmos.*, 116, D09301, doi:10.1029/2010JD015099, 2011.
- Liu, P. S. K., Deng, R., Smith, K. A., Williams, L. R., Jayne, J. T., Canagaratna, M. R., Moore, K., Onasch, T. B., Worsnop, D. R., and Deshler, T.: Transmission efficiency of an aerodynamic focusing lens system: Comparison of model calculations and laboratory measurements for the aerodyne aerosol mass spectrometer, *Aerosol Sci. Tech.*, 41, 721–733, 2007.
- Liu, S., Russell, L. M., Day, D. A., Zhao, Y., and Goldstein, A. H.: Secondary organic aerosol formation from three sources dominated summertime organic mass at Bakersfield, in preparation, 2012.
- Lohmann, U. and Feichter, J.: Global indirect aerosol effects: a review, *Atmos. Chem. Phys.*, 5, 715–737, doi:10.5194/acp-5-715-2005, 2005.
- Matthew, B. M., Middlebrook, A. M., and Onasch, T. B.: Collection efficiencies in an aerodyne aerosol mass spectrometer as a function of particle phase for laboratory generated aerosols, *Aerosol Sci. Tech.*, 42, 884–898, 2008.
- Middlebrook, A. M., Bahreini, R., Jimenez, J. L., and Canagaratna, M. R.: Evaluation of composition-dependent collection efficiencies for the aerodyne aerosol mass spectrometer using field data, *Aerosol Sci. Tech.*, 46, 258–271, 2012.
- Murphy, D. M. and Thomson, D. S.: Laser ionization mass-spectroscopy of single aerosol particles, *Aerosol Sci. Tech.*, 22, 237–249, 1995.
- Ng, N. L., Canagaratna, M. R., Zhang, Q., Jimenez, J. L., Tian, J., Ulbrich, I. M., Kroll, J. H., Docherty, K. S., Chhabra, P. S., Bahreini, R., Murphy, S. M., Seinfeld, J. H., Hildebrandt, L., Donahue, N. M., DeCarlo, P. F., Lanz, V. A., Prévôt, A. S. H., Dinar, E., Rudich, Y., and

**Organics typed by  
single particle  
measurements**

S. Liu et al.

Title Page

Abstract

Introduction

Conclusions

References

Tables

Figures

◀

▶

◀

▶

Back

Close

Full Screen / Esc

Printer-friendly Version

Interactive Discussion



Worsnop, D. R.: Organic aerosol components observed in Northern Hemispheric datasets from Aerosol Mass Spectrometry, *Atmos. Chem. Phys.*, 10, 4625–4641, doi:10.5194/acp-10-4625-2010, 2010.

5 Noble, C. A. and Prather, K. A.: Real-time measurement of correlated size and composition profiles of individual atmospheric aerosol particles, *Environ. Sci. Technol.*, 30, 2667–2680, 1996.

Phares, D. J., Rhoads, K. P., and Wexler, A. S.: Performance of a single ultrafine particle mass spectrometer, *Aerosol Sci. Tech.*, 36, 583–592, 2002.

10 Pope, C. A., Burnett, R. T., Thurston, G. D., Thun, M. J., Calle, E. E., Krewski, D., and Godleski, J. J.: Cardiovascular mortality and long-term exposure to particulate air pollution – epidemiological evidence of general pathophysiological pathways of disease, *Circulation*, 109, 71–77, 2004.

15 Quinn, P. K., Bates, T. S., Coffman, D., Onasch, T. B., Worsnop, D., Baynard, T., de Gouw, J. A., Goldan, P. D., Kuster, W. C., Williams, E., Roberts, J. M., Lerner, B., Stohl, A., Pettersson, A., and Lovejoy, E. R.: Impacts of sources and aging on submicrometer aerosol properties in the marine boundary layer across the gulf of maine, *J. Geophys. Res.-Atmos.*, 111, D23S36, doi:10.1029/2006JD007582, 2006.

20 Ramanathan, V., Crutzen, P. J., Lelieveld, J., Mitra, A. P., Althausen, D., Anderson, J., Andreae, M. O., Cantrell, W., Cass, G. R., Chung, C. E., Clarke, A. D., Coakley, J. A., Collins, W. D., Conant, W. C., Dulac, F., Heintzenberg, J., Heymsfield, A. J., Holben, B., Howell, S., Hudson, J., Jayaraman, A., Kiehl, J. T., Krishnamurti, T. N., Lubin, D., McFarquhar, G., Novakov, T., Ogren, J. A., Podgorny, I. A., Prather, K., Priestley, K., Prospero, J. M., Quinn, P. K., Rajeev, K., Rasch, P., Rupert, S., Sadourny, R., Satheesh, S. K., Shaw, G. E., Sheridan, P., and Valero, F. P. J.: Indian ocean experiment: An integrated analysis of the climate forcing and effects of the great indo-asian haze, *J. Geophys. Res.-Atmos.*, 106, 28371–28398, 2001.

25 Stein, S. E. and Scott, D. R.: Optimization and testing of mass-spectral library search algorithms for compound identification, *J. Am. Soc. Mass Spectrom.*, 5, 859–866, 1994.

30 Su, Y. X., Sipin, M. F., Furutani, H., and Prather, K. A.: Development and characterization of an aerosol time-of-flight mass spectrometer with increased detection efficiency, *Anal. Chem.*, 76, 712–719, 2004.

**Organics typed by  
single particle  
measurements**

S. Liu et al.

[Title Page](#)[Abstract](#)[Introduction](#)[Conclusions](#)[References](#)[Tables](#)[Figures](#)[◀](#)[▶](#)[◀](#)[▶](#)[Back](#)[Close](#)[Full Screen / Esc](#)[Printer-friendly Version](#)[Interactive Discussion](#)

Sullivan, R. C., Guazzotti, S. A., Sodeman, D. A., and Prather, K. A.: Direct observations of the atmospheric processing of Asian mineral dust, *Atmos. Chem. Phys.*, 7, 1213–1236, doi:10.5194/acp-7-1213-2007, 2007.

Takahama, S., Gilardoni, S., Russell, L. M., and Kilcoyne, A. L. D.: Classification of multiple types of organic carbon composition in atmospheric particles by scanning transmission X-ray microscopy analysis, *Atmos. Environ.*, 41, 9435–9451, 2007.

Thomson, D. S., Schein, M. E., and Murphy, D. M.: Particle analysis by laser mass spectrometry *wb-57f* instrument overview, *Aerosol Sci. Tech.*, 33, 153–169, 2000.

Ulbrich, I. M., Canagaratna, M. R., Zhang, Q., Worsnop, D. R., and Jimenez, J. L.: Interpretation of organic components from Positive Matrix Factorization of aerosol mass spectrometric data, *Atmos. Chem. Phys.*, 9, 2891–2918, doi:10.5194/acp-9-2891-2009, 2009.

Wieser, P., Wurster, R., and Seiler, H.: Identification of airborne particles by laser-induced mass-spectroscopy, *Atmos. Environ.*, 14, 485–494, 1980.

Zelenyuk, A., Yang, J., Choi, E., and Imre, D.: Splat II: An aircraft compatible, ultra-sensitive, high precision instrument for in-situ characterization of the size and composition of fine and ultrafine particles, *Aerosol Sci. Tech.*, 43, 411–424, 2009.

Zhang, Q., Alfarra, M. R., Worsnop, D. R., Allan, J. D., Coe, H., Canagaratna, M. R., and Jimenez, J. L.: Deconvolution and quantification of hydrocarbon-like and oxygenated organic aerosols based on aerosol mass spectrometry, *Environ. Sci. Technol.*, 39, 4938–4952, 2005.

Title Page

Abstract

Introduction

Conclusions

References

Tables

Figures

◀

▶

◀

▶

Back

Close

Full Screen / Esc

Printer-friendly Version

Interactive Discussion

**Table 1.** Comparison of single-particle measurement techniques and their detection limits.

Technique	Measured components	Size DL (nm)		Size resolution	Method for DL determination	Reference	
		$d_{va}$	$d_g$				
Laser ablation	LAMMA	–	500	–	Not specified	Wieser et al. (1980)	
	ATOFMS	200	–	25–40 nm <sup>a</sup>	Smallest laboratory-calibrated particles	Noble and Prather (1996); Gard et al. (1997)	
	UF-ATOFMS	100	–	–	Smallest particles that have non-zero detection efficiency	Su et al. (2004)	
	PALMS	–	200	–	Not specified	Murphy and Thomson, (1995); Thomason et al. (2000)	
	RSMS-III	Refractory and nonrefractory components, including organics, salts, metals, and dusts in single particles	50	–	5–20 nm <sup>b</sup>	Smallest particles that have non-zero detection efficiency	Lake et al. (2003); Johnston and Wexler (1995); Phares et al. (2002)
	SPLAT-II	–	50	–	–	Smallest particles that have non-zero detection efficiency	Zelenyuk et al. (2009)
Electron microscopy	SEM-EDX or ESEM	–	100	–	Smallest particles tested in the laboratory	Laskin et al. (2001)	
	STXM	–	100	–	Smallest particles analyzed	Takahama et al. (2007)	
Thermal volatilization	LS-Q-AMS	–	180	5–10 <sup>c</sup>	Smallest particles that have non-zero detection efficiency	Cross et al. (2007)	
	LS-ToF-AMS	Nonrefractory organics, sulfate, nitrate, ammonium, chloride of single and ensemble particles	180	130	5–10 <sup>c</sup>	Smallest particles that produce significant optical ( $S/N \geq 5$ ) and chemical signals (>100 ions)	This study
	LS-ToF-AMS	–	430	307	5–10 <sup>c</sup>	Size at which 50% of particle number are detected (compared to DMA)	This study

<sup>a</sup> Calculated as the standard deviation of the size-calibration curve fitting.<sup>b</sup> Inferred from reported size distributions.<sup>c</sup> Calculated as  $d/\Delta d$  at FWHM (full width at half maximum).

**Organics typed by  
single particle  
measurements**

S. Liu et al.

[Title Page](#)[Abstract](#)[Introduction](#)[Conclusions](#)[References](#)[Tables](#)[Figures](#)[Back](#)[Close](#)[Full Screen / Esc](#)[Printer-friendly Version](#)[Interactive Discussion](#)**Table 2.** Particle number and number fraction for the three vaporization types.

Particle vaporization type	Particle number	Number fraction (%)
Prompt	130 361	46
Delayed	16 996	6
Null	124 284	48

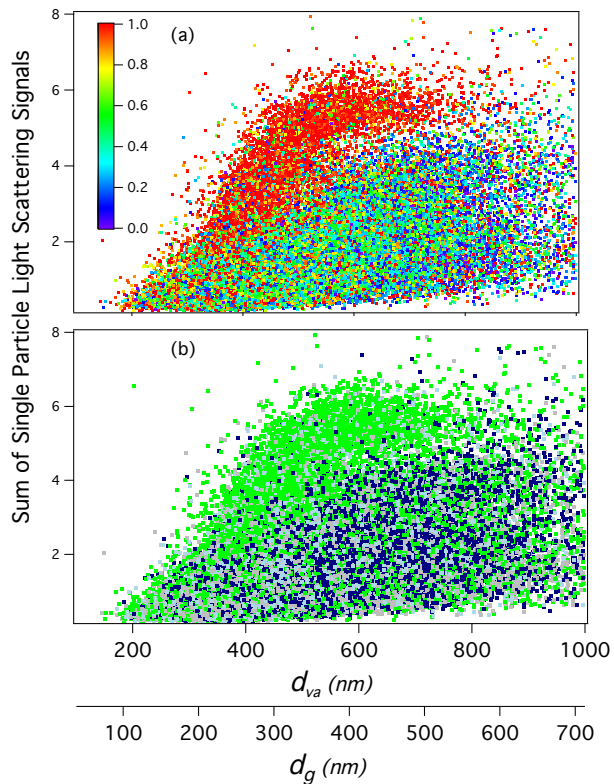


**Fig. 1.** Sum of light scattering signals of prompt and delayed particles as a function of  $d_{va}$  ( $d_g$ ). In **(a)**, each particle is colored by its organic mass fraction with colors shown in the color bar. In **(b)**, particles are colored by particle clusters derived cluster analysis in Sect. 3.2. Colors indicate Cluster I (dark blue), Cluster II (light blue), Cluster III (green), and unknown (grey).

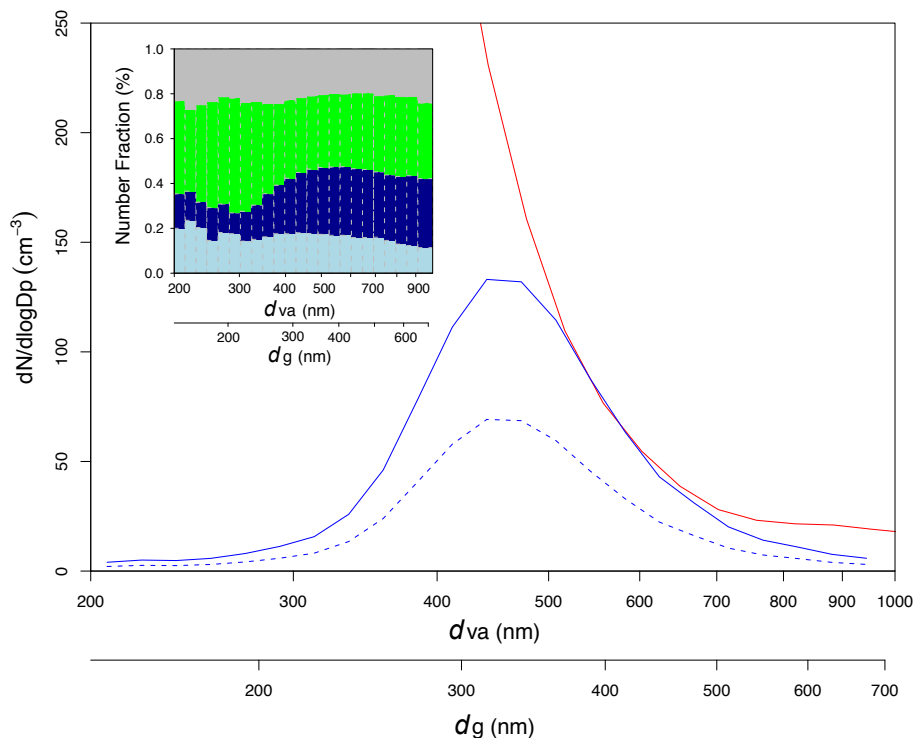


**Fig. 2.** Particle number size distributions measured by DMA (red) and LS-ToF-AMS (solid blue). A density of  $1.4 \text{ g cm}^{-3}$  was used to convert DMA mobility diameter to  $d_{va}$  (Ahlm et al., 2012). Dashed blue line represents number size distribution for sum of prompt and delayed particles. The inset shows number fractions for Cluster I (dark blue), Cluster II (light blue), Cluster III (green), and unknown (grey) particles. Particle size is binned logarithmically. For each size bin, logarithmic ratio of upper size to lower size is 0.03.

Title Page

Abstract

Introduction

Conclusions

References

Tables

Figures

⏪

⏩

◀

▶

Back

Close

Full Screen / Esc

Printer-friendly Version

Interactive Discussion



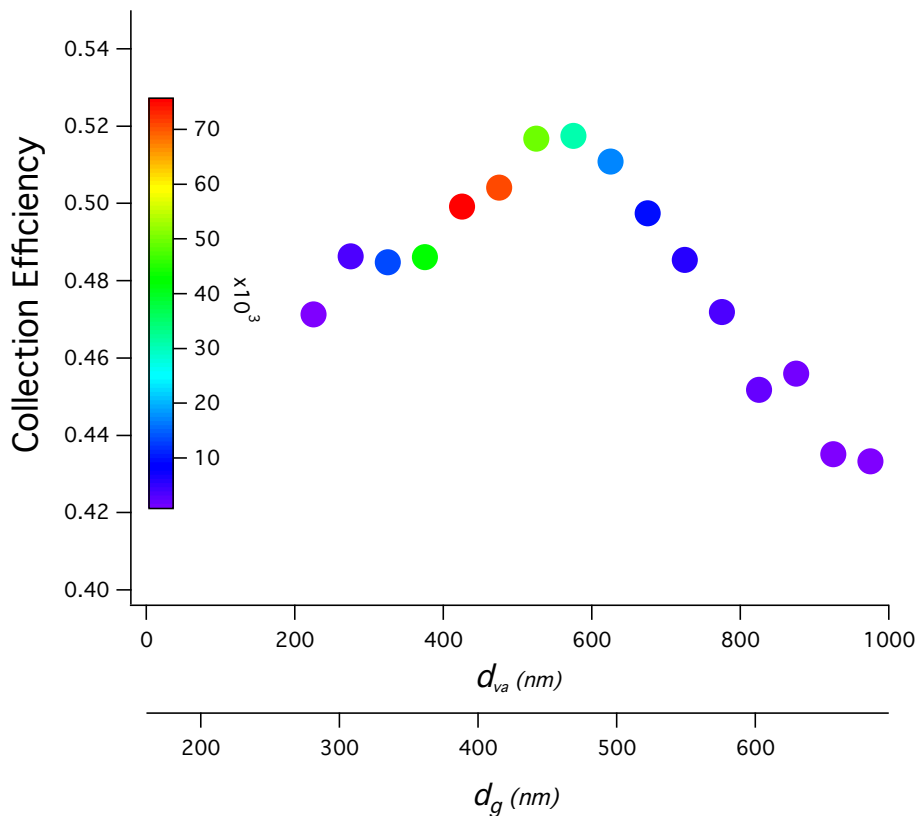


**Fig. 3.** Collection efficiency versus particle size. Point colors indicate number of particles measured in the corresponding size, with color scale shown by the vertical bar.

**Organics typed by  
single particle  
measurements**

S. Liu et al.

Title Page

Abstract Introduction

Conclusions References

Tables Figures

◀ ▶

◀ ▶

Back Close

Full Screen / Esc

Printer-friendly Version

Interactive Discussion



Organics typed by  
single particle  
measurements

S. Liu et al.

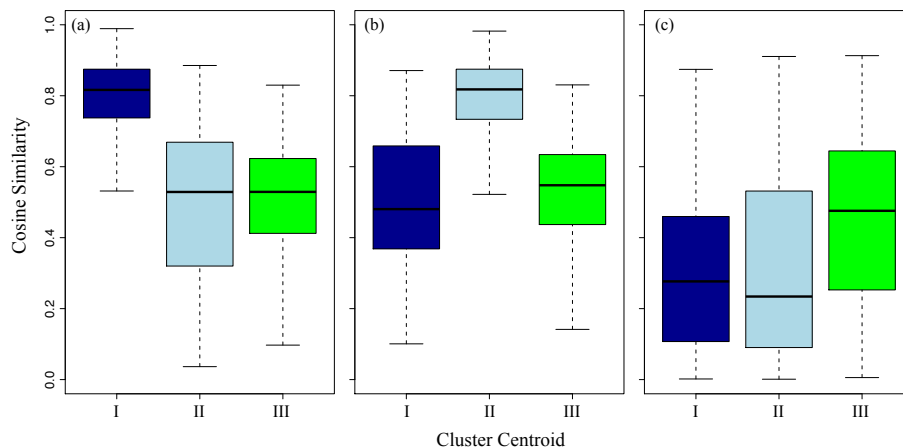


**Fig. 4.** Spectrum similarity to Cluster I centroid (dark blue), Cluster II centroid (light blue), and Cluster III centroid (green) for **(a)** Cluster I spectra, **(b)** Cluster II spectra, and **(c)** Cluster III spectra. The horizontal bar in each box represents the median value. Each box's upper and lower bounds represent the 25th and the 75th percentiles, respectively, with the whiskers extending 1.5 interquartile ranges.

[Title Page](#)[Abstract](#)[Introduction](#)[Conclusions](#)[References](#)[Tables](#)[Figures](#)[◀](#)[▶](#)[◀](#)[▶](#)[Back](#)[Close](#)[Full Screen / Esc](#)[Printer-friendly Version](#)[Interactive Discussion](#)

**Organics typed by  
single particle  
measurements**

S. Liu et al.

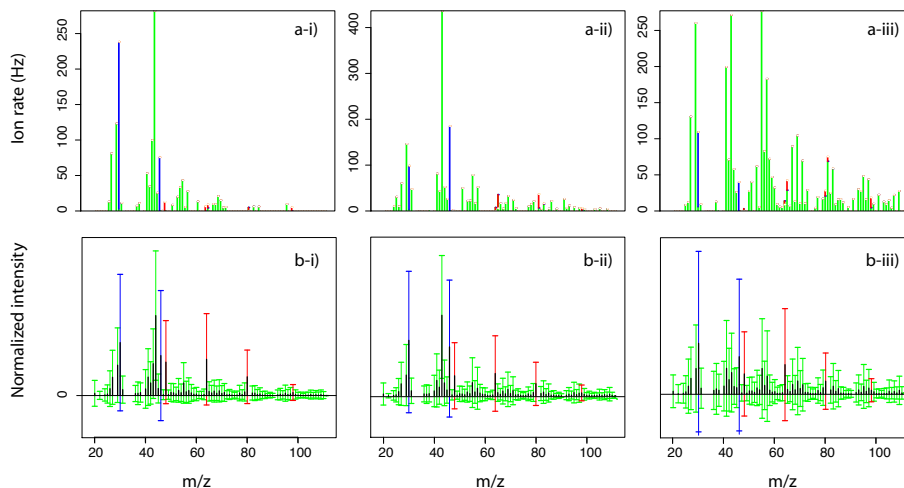


**Fig. 5.** (a) Example single-particle spectra for (i) Cluster I, (ii) Cluster II, and (iii) Cluster III. The particles in (i), (ii), and (iii) were collected on 16 May ( $d_{va} = 507$  nm,  $d_g = 362$  nm), 31 May ( $d_{va} = 402$  nm,  $d_g = 287$  nm), and 16 May ( $d_{va} = 492$  nm,  $d_g = 351$  nm), respectively. (b) Variability of normalized single-particle spectra for each cluster for this study (15 May to 29 June 2010). In each panel, the black sticks show the average spectrum for the cluster, and the whiskers represent standard deviations (variability) at each  $m/z$ . Colors indicate organic (green), nitrate (blue), and sulfate (red) fragments.

Title Page

Abstract

Introduction

Conclusions

References

Tables

Figures

◀

▶

◀

▶

Back

Close

Full Screen / Esc

Printer-friendly Version

Interactive Discussion



Organics typed by  
single particle  
measurements

S. Liu et al.

Title Page

Abstract

Introduction

Conclusions

References

Tables

Figures

◀

▶

◀

▶

Back

Close

Full Screen / Esc

Printer-friendly Version

Interactive Discussion

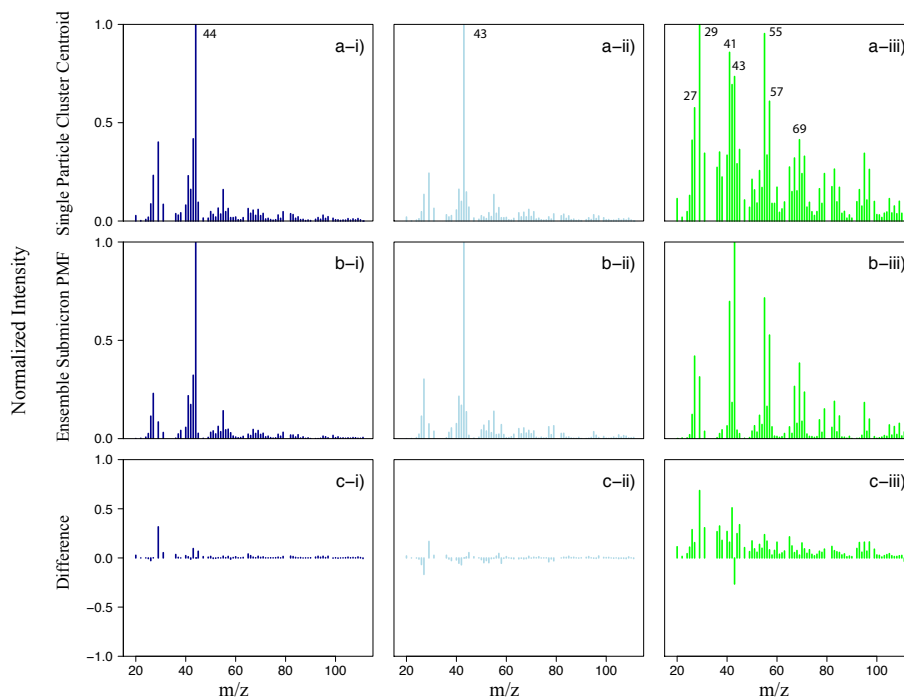


**Fig. 6.** (a) Cluster centroid (group-average mass spectrum) for (i) Cluster I, (ii) Cluster II, and (iii) Cluster III particles. (b) Mass spectrum for (i) the high O/C alkane SOA factor, (ii) the low O/C alkane SOA factor, and (iii) mass-weighted average for the COA, PO SOA, and nighttime OA factors identified from the ensemble measurements using PMF analysis. (c) The difference between spectra in (a) and (b).

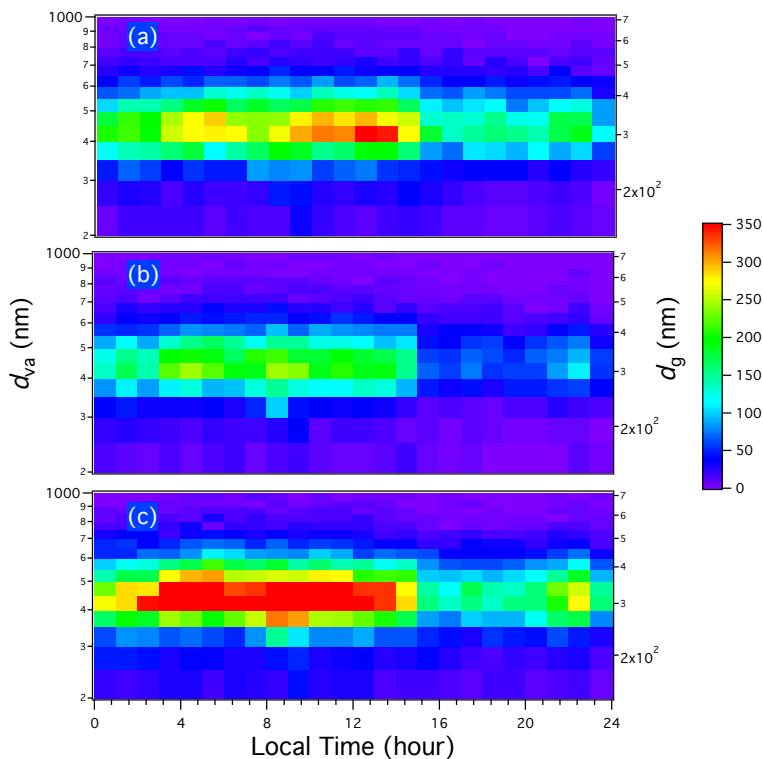


**Fig. 7.** Diurnal variations of particle number size distributions for **(a)** Cluster I, **(b)** Cluster II, and **(c)** Cluster III particles. The color bar indicates particle number. Note that LS-ToF-AMS detection efficiency for particles smaller than 400-nm  $d_{va}$  (285-nm  $d_g$ ) is much lower than for larger particles, as shown in Fig. 2. For example, number concentration of 200-nm  $d_{va}$  (140-nm  $d_g$ ) particles measured by LS-ToF-AMS was less than 1% that measured by DMA.

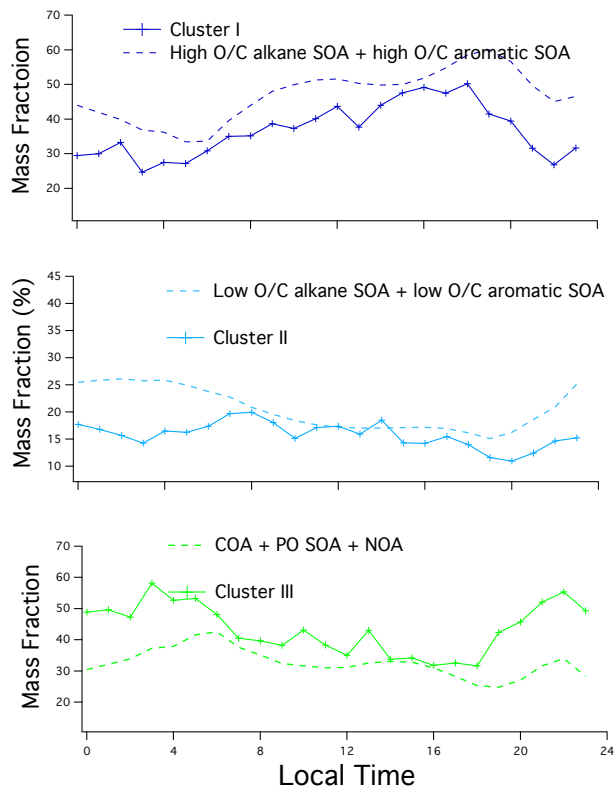


**Fig. 8.** Solid lines (with markers) show campaign average diurnal cycles of mass fraction for **(a)** Cluster I (dark blue), **(b)** Cluster II (light blue), and **(c)** Cluster III (green) particles. Dashed lines represent diurnal cycles of the mass fraction for **(a)** the sum of high O/C alkane and aromatic SOA (dark blue), **(b)** the sum of low O/C alkane and aromatic SOA (light blue), and **(c)** the sum of COA, PO SOA, and NOA factors (green) identified from ensemble measurements using PMF analysis (Liu et al., 2012). Measurements were averaged hourly.